INL/CON-16-38952
PREPRINT

Using Directional Diffusion Coefficients for Nonlinear Diffusion Acceleration of the First Order S_N Equations in Near-Void Regions

2016 ANS Winter Meeting and Nuclear Technology Expo

Sebastian Schunert, Hans Hammer, Jijie Lou, Yaqi Wang, Javier Ortensi, Frederick Gleicher, Benjamin Baker, Mark DeHart, Richard Martineau

November 2016

The INL is a
U.S. Department of Energy
National Laboratory
operated by
Battelle Energy Alliance

Using Directional Diffusion Coefficients for Nonlinear Diffusion Acceleration of the First Order S_N Equations in Near-Void Regions

Sebastian Schunert[1*], Hans Hammer[2], Jijie Lou[2] , Yaqi Wang[1], Javier Ortensi[3], Frederick Gleicher [3], Benjamin Baker [3], Mark DeHart[3], Richard Martineau[4]

[1]*Nuclear Methods Development, Idaho National Laboratory, Idaho Falls, ID, USA*
[2] *Department of Nuclear Engineering, Texas A&M University, College Station, TX, USA*
[3]*Reactor Physics Analysis & Design, Idaho National Laboratory, Idaho Falls, ID, USA*
[4] *Nuclear Science & Technology, Modeling and Simulation, Idaho National Laboratory, Idaho Falls, ID, USA*
[*]*Corresponding author: sebastian.schunert@inl.gov*

INTRODUCTION

The common definition of the diffusion coefficient as the inverse of three times the transport cross section is not compatible with voids. Morel introduced a non-local tensor diffusion coefficient that remains finite in voids [1]. It can be obtained by solving an auxiliary transport problem without scattering or fission. Larsen and Trahan successfully applied this diffusion coefficient for enhancing the accuracy of diffusion solutions of very high temperature reactor (VHTR) problems that feature large, optically thin channels in the z-direction [2]. It was demonstrated that a significant reduction of error can be achieved in particular in the optically thin region. Along the same line of thought, non-local diffusion tensors have been applied to modeling the TREAT reactor confirming the findings of Larsen and Trahan [3].

Previous work of the authors have introduced a flexible Nonlinear-Diffusion Acceleration (NDA) method for the first order S_N equations discretized with the discontinuous finite element method (DFEM), [4], [5], [6]. This NDA method uses a scalar diffusion coefficient in the low-order system that is obtained as the flux weighted average of the inverse transport cross section. Hence, it suffers from very large and potentially unbounded diffusion coefficients in the low order problem. However, it was noted that the choice of the diffusion coefficient does not influence consistency of the method at convergence and hence the diffusion coefficient is essentially a free parameter. The choice of the diffusion coefficient does, however, affect the convergence behavior of the nonlinear diffusion iterations.

Within this work we use Morel's non-local diffusion coefficient in the aforementioned NDA formulation in lieu of the flux weighted inverse of three times the transport cross section. The goal of this paper is to demonstrate that significant enhancement of the spectral properties of NDA can be achieved in near void regions. For testing the spectral properties of the NDA with non-local diffusion coefficients, the periodical horizontal interface problem is used [7]. This problem consists of alternating stripes of optically thin and thick materials both of which feature scattering ratios close to unity.

THE NONLINEAR DIFFUSION ACCELERATION METHOD

The original form of the NDA method for solving the multigroup, first order S_N eigenvalue equations is briefly introduced. This method closely follows the description in Ref. [6]. The FEM weak form of the first-order, multigroup, S_N equations is:

$$B\left(\Psi,\Psi^*\right)-R\left(\Psi,\Psi^*\right)-S\left(Q_s,\Phi^*\right)=\frac{1}{k}F\left(Q_f,\Phi^*\right), \quad (1)$$

with the bilinear forms being defined as:

$$\begin{aligned}
B\left(\Psi,\Psi^*\right)&=\sum_{g=1}^{G}\sum_{m=1}^{M}w_m\Big(\Big(\Psi_{g,m},\left(-\boldsymbol{\Omega}_m\cdot\nabla+\Sigma_{t,g}\right)\Psi^*_{g,m}\Big)_{\mathcal{D}}\\
&\quad-\left\langle\Psi^-_{g,m},[\![\Psi^*_{g,m}]\!]\right\rangle_{\Gamma}\Big)\\
R\left(\Psi,\Psi^*\right)&=\sum_{g=1}^{G}\sum_{E\in\partial D^r}\sum_{\boldsymbol{\Omega}\cdot\boldsymbol{n}>0}w_m\left\langle\Psi_{g,m},\Psi^*_{g,m^r}\right\rangle_E\\
S\left(Q_s,\phi^*\right)&=\frac{1}{4\pi}\sum_{g=1}^{G}\sum_{g'=1}^{G}\left(Q_{s,g',g},\Phi^*_g\right)_{\mathcal{D}}\\
F\left(Q_f,\phi^*\right)&=\frac{1}{4\pi}\sum_{g=1}^{G}\sum_{g'=1}^{G}\left(Q_{f,g',g},\Phi^*_g\right)_{\mathcal{D}},
\end{aligned} \quad (2)$$

In Eqs. 1 and 2 standard transport notation is used stressing in particular that g is a fine energy group index running from 1 to G; the quantities $Q_{s,g',g}$ and $Q_{f,g',g}$ will be specified later. In addition, Φ^* is an arbitrary, angularly isotropic test function, E is an FEM element's face, $\boldsymbol{n}$ is an arbitrarily oriented normal vector on E (outward normal vector on $\partial\mathcal{D}$), f^+ and f^- are upwind and downwind values of f, respectively, Γ is the set of all interior faces, $[\![f]\!]=f^+-f^-$ is the jump across an element's face with the upwind and downwind sides being defined by $\boldsymbol{\Omega}_m$, and

$$(f,g)_{\mathcal{D}} = \int_{\mathcal{D}} dV f g \quad (3)$$

$$\langle f,g\rangle_E = \int_E dA\,|\boldsymbol{\Omega}_m\cdot\boldsymbol{n}|\,fg. \quad (4)$$

It is noted that all quantities related to the S_N problem are denoted in capitalized symbols, e.g. $\Sigma_{t,g}$, and all quantites related to the diffusion problem are denoted by lower case symbols with the exception of the diffusion coefficient. The weak form of the interior penalty DFEM diffusion equations is given by:

$$b\left[\Psi\right]\left(\phi,\phi^*\right)+c\left[\Psi\right]\left(\phi,\phi^*\right)=\frac{1}{k}f\left[\Psi\right]\left(\phi,\phi^*\right), \quad (5)$$

where the dependence on the S_N transport solution is denoted by the square bracket, and

$$
\begin{aligned}
b\left[\Psi\right](\phi,\phi^*) &= \sum_{p=1}^{P}(\hat{D}_p\boldsymbol{\nabla}\phi_p,\boldsymbol{\nabla}\phi_p^*)_{\mathcal{D}} + \sum_{p=1}^{P}(\sigma_{r,p}\phi_p,\phi_p^*)_{\mathcal{D}} \\
&- \sum_{p=1}^{P}\sum_{p'\neq p}(\sigma_s^{p'\to p}\phi_{p'},\phi_p^*)_{\mathcal{D}} + \sum_{p=1}^{P}(\{\hat{D}_p\boldsymbol{\nabla}\phi_p\cdot\boldsymbol{n}\},[\![\phi_p^*]\!])_{\Gamma} \\
&+ \sum_{p=1}^{P}(\kappa_p[\![\phi_p]\!],[\![\phi_p^*]\!])_{\Gamma} \\
f\left[\Psi\right](\phi,\phi^*) &= \sum_{p=1}^{P}\sum_{p'=1}^{P}(\chi_p\nu\sigma_{f,p'}\phi_{p'},\phi_p^*)_{\mathcal{D}} \qquad (6)
\end{aligned}
$$

where p is the coarse group index, P is the total number of coarse energy groups, $\hat{D}_p$ is the diffusion coefficient, $\sigma_{r,p}$ is the removal cross section, κ_p is the penalty parameter, $[\![f]\!] = f^+ - f^-$ is the jump across an element's face with the upwind and downwind side being defined by the face's normal vector (normal vector $\boldsymbol{n}$ points from − to +), $\{f\} = \frac{1}{2}(f^+ + f^-)$. For details on the utilized quantities consult Ref. [6]. The closure term $c\left[\Psi\right](\phi,\phi^*)$ is defined as:

$$
\begin{aligned}
c\left[\Psi\right](\phi,\phi^*) &= \sum_{p=1}^{P}(\hat{D}_p\phi_p,\boldsymbol{\nabla}\phi_p^*)_{\mathcal{D}} + \sum_{p=1}^{P}([\![\hat{\kappa}_p\phi_p]\!],[\![\phi_p^*]\!])_{\Gamma} \\
&+ \sum_{p=1}^{P}(\frac{\alpha_p}{4}\phi_p,\phi_p^*)_{\mathcal{D}^s}, \qquad (7)
\end{aligned}
$$

where $\hat{D}_p$ is the drift vector, $\hat{\kappa}_p$ is the face closure, and α_p is the boundary coefficient. Definitions of these parameter are provided in Ref. [6]. The diffusion coefficient is computed as the flux weighted inverse of the transport cross section:

$$
\hat{D}_p = \frac{\Pi\left[\frac{1}{3\Sigma_{tr,g}}\Phi_g\right]}{\Pi\left[\Phi_g\right]}\hat{I}, \qquad (8)
$$

where $\hat{I}$ is the identity matrix, $\Pi\left[\cdot\right]$ denotes the projection operator defined in Ref. [6]. The scalar diffusion coefficient defined by Eq. 8 becomes unbounded in void regions and destroys effectiveness of the NDA method in optically thin regions. Finally, the update of the S_N equations is given by

$$
\begin{aligned}
Q_{s,g',g} &= \Sigma_s^{g'\to g}\Phi_{g'}^p \\
Q_{f,g',g} &= K_g\nu\Sigma_{f,g'}\Phi_{g'}^p \\
\Phi_g^p &= \Phi_{g'} + \Pi^{-1}\left[\phi_p - \Pi\left[\Phi_g\right]\right], \qquad (9)
\end{aligned}
$$

where Φ_g is the S_N transport scalar flux, K_g is the fission spectrum and $\Pi^{-1}\left[\cdot\right]$ is the prolongation operator defined in [6].

Morel's non-local diffusion diffusion tensor is obtained as the solution of the simple linear transport problem [1]:

$$
\begin{aligned}
\hat{\Omega}\cdot\nabla F_{g,m}(\boldsymbol{r}) + \Sigma_{t,g}F_{g,m} &= 1,\ m = 1,..,M \\
\hat{D}_{g,i,j}(\boldsymbol{r}) &= \frac{1}{4\pi}\sum_{m=1}^{M} w_m\hat{\Omega}_{m,i}\hat{\Omega}_{m,j}F_{g,m},\ i,j = x,y,z. \\
\hat{D}_{p,i,j} &= \Pi\left[\hat{D}_{g,i,j}\right]. \qquad (10)
\end{aligned}
$$

Following Ref. [2] reflective boundary conditions are applied on all exterior boundaries unless stated otherwise ensuring that in the limit of a homogeneous medium with finite total cross section, the scalar diffusion coefficient $1/3\Sigma_{t,g}$ is obtained. The auxiliary transport problem Eq. 10 is discretized using the same discretization in space and angle as the solution of the primary transport problem. However, it is noted that high accuracy of the tensor diffusion coefficients might not be necessary for rendering an effective NDA algorithm. Further, Eq. 10 constitutes a system of decoupled, linear transport problems that can be solved using a single transport sweep if we neglect the reflective boundary conditions. Depending on the optical thickness of the domain, a small number of transport sweeps might be necessary to obtain the solution of Eq. 10 in case reflective boundary conditions are applied.

Within this work, we replace the scalar diffusion coefficients Eq. 8 by the tensor diffusion coefficients defined by Eq. 10. The resulting NDA algorithm listed in Alg. 1 is implemented into the radiation transport code Rattlesnake [8]. The tensor diffusion coefficients are pre-computed before commencing Picard iterations solving the NDA system of equations as they only depend on the supplied cross sections and the geometry neither of which change during the solution of the presented test problems. In general multi-physics settings, it would be necessary to recompute the $\hat{D}_{g,i,j}$ whenever feedback from other physics changes $\Sigma_{t,g}$.

Algorithm 1 Nonlinear diffusion acceleration algorithm with non-local tensor diffusion coefficients.

Solve Eq. 10 and transfer $\hat{D}_{g,i,j}$ to the diffusion problem.
Set $l = 0$, $\Psi^l = 1$.
while $\epsilon > tol$ **do**
1. Project Ψ^l, i.e. compute $\Pi\Psi^l$, and compute low order cross sections.
2. Obtain $\phi^{l+1/2}$ by solving the low order eigenvalue/fixed source problem using MOOSE's *NonlinearEigen/PJFNK* solver capability.
3. Prolongation, i.e. evaluate $\boldsymbol{\Pi}^{-1}\left[\phi^{l+1/2} - \boldsymbol{\Pi}\Phi^l\right]$.
4. Obtain Ψ^{l+1} by performing a single transport sweep.
5. Compute Φ^{l+1}.
6. $\epsilon = \|1 - \Phi^{l+1}/\Phi^l\|_2$, $l = l + 1$.

end while

NUMERICAL RESULTS

The periodical horizontal interface (PHI) problem is a well-known litmus test for numerical methods [7]. It consists of alternating horizontal stripes of optically thin and thick materials of thickness 1 cm as depicted in Fig. 1 with one-group total and scattering cross sections given by:

$$
\begin{aligned}
\Sigma_{t,R1} &= \tau \\
\Sigma_{s,R1} &= c\Sigma_{t,R1} \\
\Sigma_{t,R2} &= \frac{1}{\tau} \\
\Sigma_{s,R2} &= c\Sigma_{t,R2}, \qquad (11)
\end{aligned}
$$

where the two parameter τ and the scattering ratio c are varied during the following parameter study. The parameter τ controls the material discontinuity at the interface of regions one and two, while c controls the relative amounts of scattering and absorption. The domain size is kept fixed at 11×11 cm and it is discretized using a uniform quadrilaterial mesh with 11 by 11 elements. Vacuum boundary conditions are applied on all exterior boundaries. It should be pointed out that these boundary conditions can differ from the boundary conditions applied to the auxiliary transport problem Eq. 10. Note that in this setup the optically thin regions are adjacent to the bottom and top boundaries. The S_N equations are discretized using the S_8 level symmetric quadrature. A uniform distributed source of strength one is present throughout the domain.

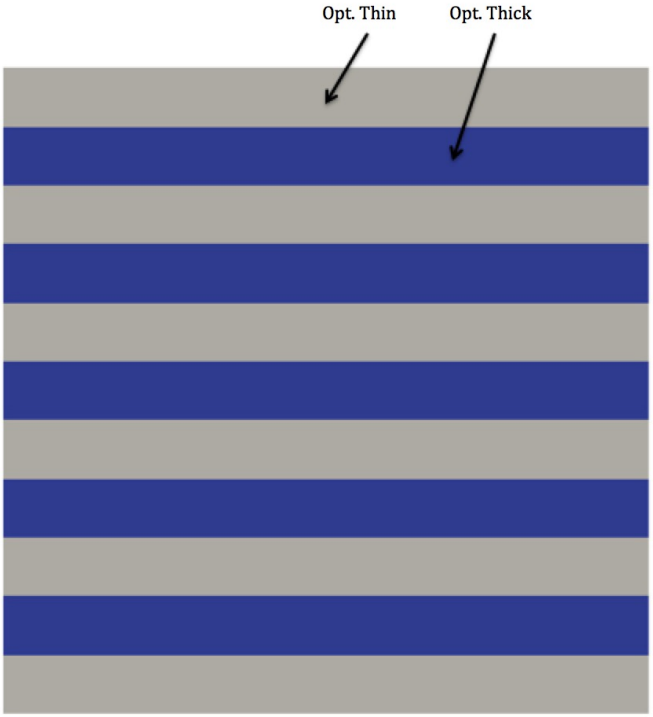

Fig. 1. Geometry of the periodical horizontal interface problem used for numerical tests of the NDA method.

Spectral radii for the PHI problem with $\log_{10}(\tau) = 1, .., 7$ and $c = 0.9, 0.99, 0.9999, 0.999999$ are listed in Tables I and II, respectively. These results demonstrate a superior performance of the non-local diffusion coefficients. For the scalar diffusion coefficients the spectral radii approach the scattering ratio c with increasing τ while for the non-local diffusion tensors, they approach a different limit that is smaller than the scattering ratio. In addition, the non-local diffusion tensor's spectral radii go through a maximum spectral radius before approaching their limit for $\tau \to \infty$. The spectral radii for the scalar diffusion coefficients increase monotonically.

The $\hat{D}_{x,x}$ and $\hat{D}_{y,y}$ components of the diffusion tensor for the case of $\tau = 1.2$ and $\tau = 1000$ are plotted in Fig. 2 and Fig. 3, respectively. While all convergence results are obtained using a uniform 11 by 11 mesh and linear discontinuous representation of the diffusion coefficients, the plots depicting the

TABLE I. Spectral radii of the NDA method obtained for the PHI problem using the flux weighted scalar diffusion coefficient.

	Scattering Ratio		
$\log_{10}(\tau)$	0.9	0.99	0.9999
0	0.27	0.30	0.3006
1	0.73	0.87	0.8826
2	0.87	0.97	0.9905
3	0.89	0.99	0.9970
4	0.9	0.99	0.9992
5	0.9	0.99	0.9998

TABLE II. Spectral radii of the NDA method obtained for the PHI problem using the non-local diffusion coefficients.

	Scattering Ratio				
$\log_{10}(\tau)$	0.9	0.99	0.9999	0.999999	1
0	0.27	0.30	0.30	0.30	0.30
1	0.56	0.64	0.63	0.63	0.63
2	0.55	0.78	0.75	0.75	0.75
3	0.49	0.74	0.80	0.78	0.78
4	0.48	0.67	0.81	0.78	0.80
5	0.48	0.66	0.75	0.81	0.80
6	0.48	0.66	0.72	0.81	0.80
7	0.48	0.66	0.71	0.75	0.80

shape of the diffusion tensor components use an 11 by 44 mesh and project the diffusion coefficients onto constant elemental shape functions. This is necessary because of limitations in the visualization procedure failing to correctly handle discontinuous shape functions with orders greater than zero. It is noted that the diffusion coefficients in both regions stay between values of 0 and 1; it is observed that the values of the $\hat{D}_{x,x}$ component are slightly larger than the $\hat{D}_{y,y}$ component. Note that x is aligned with the horizontal stripes while y is orthogonal to it. A curious behavior is observed at the bottom and top boundary where the magnitude of the diffusion coefficients is larger than in the interior. This is caused by the optically thin channels being adjacent to the reflective boundary. In the limit of $\tau \to \infty$ you can show that in slab geometry the value of the diffusion coefficients in the optically thick region becomes 0, while it approaches $\frac{1}{2}\Delta x$ where Δx is the thickness of the single stripe in the thin region. In the described geometry, we apply reflective boundary conditions at the outer boundary adjacent to an optically thin stripe making it essentially twice as large.

The behavior near the boundary prompted us to change the auxiliary transport system's boundary conditions to vacuum boundary conditions consistent with the boundary conditions used for the main transport solve. The corresponding spectral radii are listed in Table III. It is observed that the limit of the spectral radii as $\tau \to \infty$ is different than for the case with reflective boundary conditions; in particular the spectral radii are smaller rendering the NDA method more effective. It remains to be studied which boundary conditions result in the best convergence properties of the NDA method for general

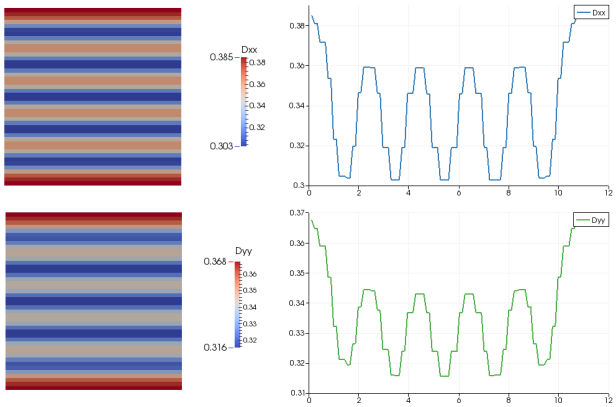

Fig. 2. Plot of the non-local diffusion coefficients $\hat{D}_{x,x}$ and $\hat{D}_{y,y}$ for $\tau = 1.2$ and reflective boundary conditions (left) and centerline plot of the diffusion coefficients (right).

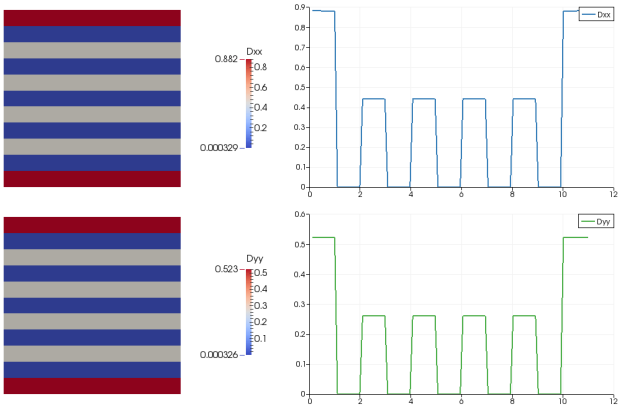

Fig. 3. Plot of the non-local diffusion coefficients $\hat{D}_{x,x}$ and $\hat{D}_{y,y}$ for $\tau = 1000.0$ and reflective boundary conditions (left) and centerline plot of the diffusion coefficients (right).

problems. In Figs. 4 and 5 the components $\hat{D}_{x,x}$ and $\hat{D}_{y,y}$ of Morel's diffusion tensor are plotted for $\tau = 1.2$ and $\tau = 1000$, respectivly. It is observed that the magnitude of the components is smaller than for the case with reflective boundary conditions. For small τ we see the characteristic drop near the vacuum boundary, while for large τ an asymptotic constant value is asymptotically approached.

In infinite, homogeneous media, the spectral radius of NDA converges to the theoretical value of 0.2247 obtained for Diffusion Synthetic Acceleration applied to the continuous transport equations when reducing the element optical thickness [7]. The thin cell limit of the spectral radii obtained with standard and non-local diffusion coefficent flavors of NDA are listed in Table IV; for creating a homogeneous medium τ is set to unity and the scattering ratio is $c = 0.9999$. Note that vacuum boundary conditions are applied such that the limit of the spectral radius is smaller than the limit in the infinite medium even for the standard diffusion coefficient. Comparing the standard and non-local methods, the limits to which the spectral radii converge with reducing the element optical thickness are distinctly different: 0.16 (non-local) compared

TABLE III. Spectral radii of the NDA method obtained for the PHI problem using the non-local diffusion coefficients, where the auxiliary problem is solved using vacuum boundary conditions.

	Scattering Ratio				
$\log_{10}(\tau)$	0.9	0.99	0.9999	0.999999	1
0	0.23	0.26	0.26	0.26	0.26
1	0.36	0.49	0.51	0.51	0.51
2	0.37	0.58	0.70	0.70	0.70
3	0.38	0.45	0.70	0.74	0.74
4	0.38	0.43	0.59	0.73	0.74
5	0.38	0.43	0.49	0.70	0.74
6	0.38	0.43	0.43	0.59	0.74
7	0.38	0.43	0.45	0.49	0.74

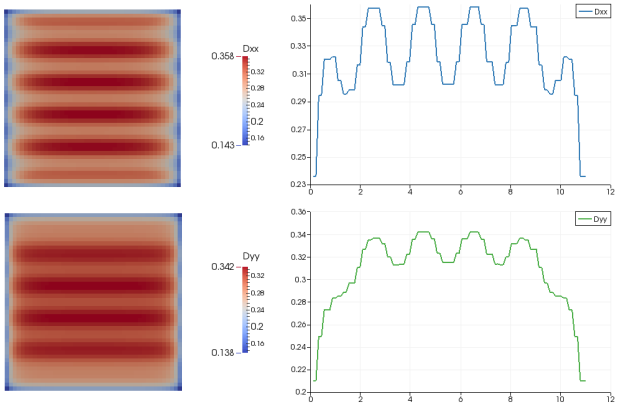

Fig. 4. Plot of the non-local diffusion coefficients $\hat{D}_{x,x}$ and $\hat{D}_{y,y}$ for $\tau = 1.2$ and vacuum boundary conditions (left) and centerline plot of the diffusion coefficients (right).

with 0.19 (standard). Note that this test is not an infinite homogeneous medium test due to the finite domain measuring 11 mean free paths across; in an infinite homogeneous medium the non-local diffusion tensor is identical to the standard diffusion coefficient and the two approaches would yield the same spectral radius equal to 0.2247.

CONCLUSIONS

In this paper we studied the convergence properties of a modification of the NDA algorithm described in [4]. Instead of using a flux weighted inverse of the transport cross sections as the diffusion coefficient, Morel's non-local tensor diffusion coefficient is utilized. The diffusion coefficient is essentially a free parameter of the NDA method that does not affect consistency as it cancels out at convergence. The goal of this modification is to improve the NDA's spectral properties in near void regions. In this work it is demonstrated that the careful choice of the diffusion coefficient is imperative for achieving good convergence properties under the said conditions. The flux-weighted scalar diffusion coefficient becomes unbounded as the optical thickness approaches zero, while Morel's non-local diffusion coefficient remains finite. Using

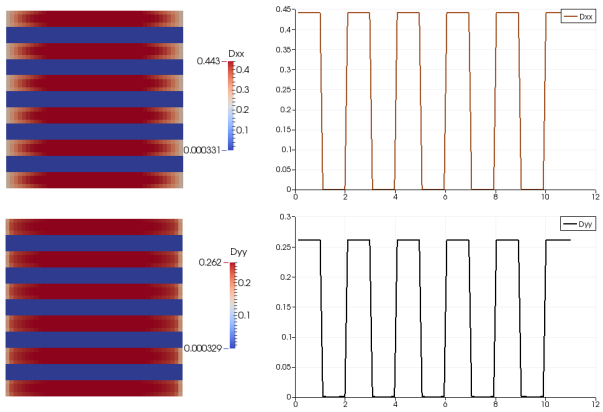

Fig. 5. Plot of the non-local diffusion coefficients $\hat{D}_{x,x}$ and $\hat{D}_{y,y}$ for $\tau = 1000.0$ and vacuum boundary conditions (left) and centerline plot of the diffusion coefficients (right).

TABLE IV. Spectral radii of the NDA method using local and non-local (using vacuum boundary conditions in the auxiliary problem) diffusion coefficients for a homogeneous medium ($\tau = 1$) with $c = 0.9999$ and varying optical cell thicknesses.

	Diffusion coefficient	
Element optical thickness	Non-local	Local
1	0.264	0.301
0.5	0.192	0.221
0.25	0.162	0.199
0.125	0.159	0.195
0.0625	0.159	0.194

the periodical horizontal interface problem as test case, it is demonstrated that the new NDA algorithm features significantly better spectral properties than the NDA algorithm with standard scalar diffusion coefficients. In particular, as the heterogeneity parameter τ is increased, the spectral radius of the original NDA method approaches the scattering ratio, while for the case with non-local diffusion coefficients it approaches a smaller limit.

ACKNOWLEDGMENTS

This manuscript has been authored by Battelle Energy Alliance, LLC under Contract No. DE-AC07-05ID14517 with the U.S. Department of Energy. The United States Government retains and the publisher, by accepting the article for publication, acknowledges that the United States Government retains a nonexclusive, paid-up, irrevocable, world-wide license to publish or reproduce the published form of this manuscript, or allow others to do so, for United States Government purposes.

REFERENCES

1. "A Non-Local Tensor Diffusion Theory," Research Report LA-UR-07-5257, Los Alamos National Laboratory, Los Alamos, NM (2007).
2. T. TRAHAN and E. LARSEN, "3-D ANISOTROPIC NEUTRON DIFFUSION IN OPTICALLY THICK MEDIA WITH OPTICALLY THIN CHANNELS," in "Proc. Int. Conf. on Mathematics and Computational Methods Applied in Nuclear Science and Engineering (MC 2011)," ANS, Rio de Janeiro, Brazil (2011).
3. J. ORTENSI, Y. WANG, B. BAKER, S. SCHUNERT, F. GLEICHER, M. DEHART, A. LAURIER, and A. HEBERT, "Preparation of a Neutron Transport Data Set for Simulations of the Transient Test Reactor Facility," in "Proc. PHYSOR 2016 Unifying Theory and Experiments in the 21st Century," ANS, Sun Valley, Idaho (2016).
4. S. SCHUNERT, Y. WANG, J. ORTENSI, F. GLEICHER, M. DEHART, and R. MARTINEAU, "A High-Order Nonlinear Diffusion Acceleration for the SN Equations Discretized with the Discontinuous FEM I: Theory and Numerical Results," *Transactions of the American Nuclear Society*, **113**, *1*, 677–679 (2015).
5. S. SCHUNERT, Y. WANG, J. ORTENSI, F. GLEICHER, M. DEHART, and R. MARTINEAU, "A High-Order Nonlinear Diffusion Acceleration for the SN Equations Discretized with the Discontinuous FEM II: Fourier Analysis," *Transactions of the American Nuclear Society*, **113**, *1*, 680–683 (2015).
6. S. SCHUNERT, Y. WANG, J. ORTENSI, F. GLEICHER, B. BAKER, M. DEHART, and R. MARTINEAU, "A Flexible Nonlinear Diffusion Acceleration Method for the First Order Eigenvalue Sn Equations Discretized with Discontinuous FEM," in "Proc. PHYSOR 2016 Unifying Theory and Experiments in the 21st Century," ANS, Sun Valley, Idaho (2016).
7. Y. WANG, H. ZHANG, and R. MARTINEAU, "Diffusion Acceleration Schemes for the Self-Adjoint Angular Flux Formulation with a Void Treatment," *Nuclear Science and Engineering*, **176**, 201–225 (2014).
8. Y. WANG, "Nonlinear Diffusion Acceleration for the Multigroup Transport Equation Discretized with S_N and Continuous FEM with Rattlesnake," in "International Conference on Mathematics and Computational Methods Applied to Nuclear Science and Engineering," Sun Valley, Idaho (May 5–9 2013), pp. 2648–2665.